Graph-Constrained Sparse Construction of Longitudinal Diffusion-Weighted Infant Atlases

Jaeil Kim, Geng Chen, Weili Lin, Pew-Thian Yap, and Dinggang Shen(✉)

Department of Radiology and BRIC,
University of North Carolina at Chapel Hill, Chapel Hill, US
dgshen@med.unc.edu

Abstract. Constructing longitudinal diffusion-weighted atlases of infant brains poses additional challenges due to the small brain size and the dynamic changes in the early developing brains. In this paper, we introduce a novel framework for constructing longitudinally-consistent diffusion-weighted infant atlases with improved preservation of structural details and diffusion characteristics. In particular, instead of smoothing diffusion signals by simple averaging, our approach fuses the diffusion-weighted images in a patch-wise manner using sparse representation with a graph constraint that encourages spatiotemporal consistency. Diffusion-weighted atlases across time points are jointly constructed for patches that are correlated in time and space. Compared with existing methods, including the one using sparse representation with $l_{2,1}$ regularization, our approach generates longitudinal infant atlases with much richer and more consistent features of the developing infant brain, as shown by the experimental results.

1 Introduction

Diffusion-weighted imaging (DWI) has been widely employed in various studies on brain development of both term and pre-term babies [1]. It is a unique technique capable of *in vivo* characterization of tissue microstructure and white matter pathways. For quantitative analysis using DWI, several diffusion-weighted (DW) atlases based on diffusion tensor imaging (DTI) [2] and higher angular resolution diffusion imaging (HARDI) [3] have been introduced. However, existing approaches to atlas construction typically average the aligned DW images, thus blurring structural details as well as diffusion properties. In this article, we focus on improving longitudinal DW infant atlases by explicit consideration of structural misalignment for constructing atlases with greater structural details.

In general, the atlas construction process consists of two steps: (1) alignment of a population of images to a common space, and (2) fusion of the aligned images into a final atlas. In recent years, effective approaches on image fusion have been introduced to preserve anatomical details. Serag *et al.* [4] employed adaptive kernel regression in the temporal dimension for construction of longitudinal T1 and T2-weighted atlases. Shi *et al.* [5] proposed a patch-wise fusion

M. Descoteaux et al. (Eds.): MICCAI 2017, Part I, LNCS 10433, pp. 49–56, 2017.
DOI: 10.1007/978-3-319-66182-7_6

method based on multi-task LASSO [6], leading to sharper atlases by fusing only patches that are representative of the image population. More recently, Zhang *et al.* [7,8] extended Shi *et al.*'s work to the frequency and temporal domains for construction of longitudinal T1-weighted atlases. Behrouz *et al.* [9] demonstrated that structural preservation in DW atlases can be improved by enforcing consistency between angular neighbors using group sparsity. This work, however, is limited to constructing atlases of a single time point.

The human brain undergoes dramatic changes in the first year of life. Dedicated method taking into account these changes is needed for effective construction of infant DW atlases. In this paper, we propose a novel approach to construct longitudinal infant DW atlases with greater details and temporal consistency. We employ sparse representation [10] with guidance by a graph that encodes the relationships between spatially and temporally neighboring patches. Experimental results indicate that the proposed method improves the quality of the DW atlases in terms of structural details and fiber coherence, compared with existing image fusion methods.

2 Method

2.1 Longitudinal Image Normalization

Our method for DW atlas construction starts with group-wise image normalization to align the DW images of each individual at each time point to an age-specific common space, and also to determine image spatial correspondences between time points. We first align the DW images of all subjects at each age using group-wise registration [11] with their fractional anisotropy (FA) maps. We reorient the diffusion signals using the method described in [12]. Then, we compute age-specific templates ($\bar{I}_t$) of aligned DW images ($I_{i,t}$) at each time point (t) using kernel regression based on age [7]:

$$\bar{I}_t = \frac{\sum_{i=1}^{N} g_{i,t} I_{i,t}}{\sum_{i=1}^{N} g_{i,t}}, \tag{1}$$

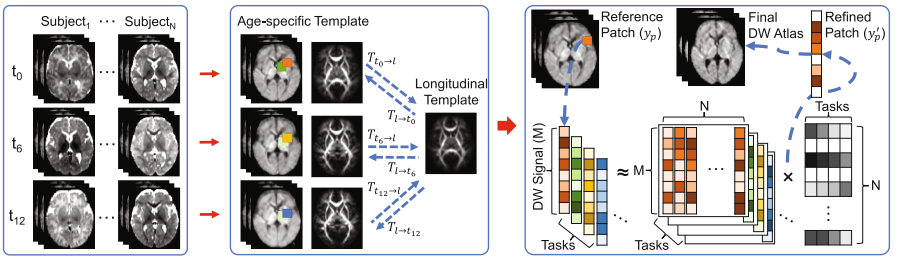

Fig. 1. Overview of longitudinal diffusion-weighted (DW) atlas construction

where $g_{i,t} = \frac{1}{\sigma\sqrt{2\pi}} \exp\left(-\frac{\left(k_{i,t}-\bar{k}_t\right)^2}{2\sigma}\right)$. $k_{i,t}$ is postnatal age at scan time, and $\bar{k}_t$ is average age of a population at t. We determine σ as standard deviation of subjects' age in the population. Next, we build a longitudinal template using group-wise registration with FA maps of the age-specific templates. Through this process, we can find spatial and temporal correspondences across different time points using the displacement maps ($T_{t\to l}$ in Fig. 1) between the age-specific templates and the longitudinal template.

2.2 Patch Fusion via Graph-Constrained Sparse Representation

We construct the DW atlases at each time point in a patch-wise manner. We define a patch as a 4D block, which includes diffusion signals of all gradient directions. This signals are normalized by the average $b = 0$ signal. The estimation of a patch of the atlas at location s and time-point t is deemed as a task (p) in multi-task learning. For each task, we first extract spatiotemporally neighboring patches from the individual images at each voxel locations and its 26-connected neighbors across time points. In this process, the age-specific templates are used as references. The age-specific template and individual DW images of different time points are transformed to the common space at time-point t beforehand. Patches from the individual images form a dictionary D_p. If we denote the reference patches from the age-specific templates as $\{y_p\}$, the goal is to find optimal sparse weights $\{w_p\}$ that minimize differences between $D_p w_p$ and y_p for all p. Each patch and its spatiotemporal neighbors are estimated jointly using multiple task learning with a spatiotemporal graph constraint (step (b) in Fig. 1). That is, we solve the following problem:

$$\begin{aligned}\hat{W} \;=\; & \underset{W}{\operatorname{argmin}} \sum_{p\in\mathbb{P}} \|y_p - D_p w_p\|^2 + \lambda_1 \|W\|_1 \\ & + \lambda_2 \sum_{p\in\mathbb{P}} \sum_{p'\in\mathbb{N}(p)} \|\alpha\,(p,p')\,(w_p - w_{p'})\,\|_2^2, \end{aligned} \tag{2}$$

where $\mathbb{P}$ is a set of all tasks for a target patch and its spatiotemporal neighbors, W is a matrix containing sparse weights for each task (w_p) as column vector, and $\mathbb{N}(p)$ is the set of tasks associated with the spatiotemporal neighbors. λ_1 is a parameter used to control the sparsity resulting from l_1 regularization (second term of Eq. (2)). λ_2 is a parameter used to control the similarity between the sparse weights for neighboring tasks. The spatiotemporal relatedness between tasks are encoded using weights $\alpha\,(p,p')$:

$$\alpha\,(p,p') \;=\; \exp\left[-\left(\frac{d_s\,(p,p')^2}{2\gamma_s^2} + \frac{d_t\,(p,p')^2}{2\gamma_t^2}\right)\right], \tag{3}$$

where $d_s\,(p,p')$ and $d_t\,(p,p')$ are spatial distance and age difference between task p and its neighbor task p', respectively. They are normalized by their maximum values. γ_s and γ_t are parameters used to control the relatedness between tasks by

scaling the spatial and temporal distances separately. The third term in Eq. (2) for the relatedness between tasks can be reformulated using a graph Laplacian L of size $q \times q$:

$$\hat{W} = \underset{W}{\operatorname{argmin}} \sum_{p \in \mathbb{P}} \| y_p - D_p w_p \|^2 + \lambda_1 \| W \|_1 + \lambda_2 \operatorname{tr}\left(WLW^T\right) \tag{4}$$

where $L = H - A$, and q is the number of all tasks (= size of $\mathbb{P}$). H is a diagonal matrix, with each diagonal element $h_{p,p}$ computed as $\sum_{p \in \mathbb{N}(p)} \alpha(p, p')$. A is an adjacency matrix with elements $\{\alpha(p, p')\}$. Using this formulation, we can enforce greater similarity constraints between tasks that are highly correlated.

3 Experiments

3.1 Materials

We demonstrate the effectiveness of our method in longitudinal DW atlas construction using dataset of an infant population (28 subjects, born at full term). For each subject, 42 diffusion-weighted images were acquired using 3T Siemens Allegra scanner with a spin-echo echo planar imaging sequence using TR/TE = 7680/82 ms, resolution = $2 \times 2 \times 2$ mm^3, and $b = 1000$ s/mm^2. Seven non-diffusion-weighted ($b = 0$) reference scans were acquired. The image dimension is $128 \times 96 \times 60$. We built the atlases for neonate, 6 and 12 months of age using the DW images of 20 subjects. Each subject has different number of longitudinal scans (1.2 scans on average). The DW images of remaining 8 subjects at three time points are used for the following evaluations. All DW images were processed using the FSL software package [13] for the correction of eddy current distortion and brain region extraction using the averaged $b = 0$ images.

3.2 Implementation Detail

The parameters of our algorithm need to be adjusted: (1) patch size, (2) the sparsity parameter (λ_1), (3) the graph constraint parameter (λ_2), and (4) the task relatedness parameters (γ_s and γ_t). In the following experiments, we fixed the patch size as $3 \times 3 \times 3 \times 42$, where 42 is the number of diffusion-weighted volumes. We set λ_1 and λ_2 as 5 that produced better details in final atlases via a grid search. We set γ_s and γ_t as 5.0 and 1.0 respectively in the same way.

3.3 Comparison with Existing Image Fusion Methods

To evaluate the effectiveness of the proposed method, we compare it with other existing fusion methods, including kernel regression based on age [4], multi-task LASSO with spatial consistency ($l_{2,1}$-Spatial) [8,9] and spatiotemporal consistency ($l_{2,1}$) [7]. Figure 2 shows the FA maps of the atlases. Compared with other methods, the proposed method provides clearer boundaries with less noise-like artifacts (see arrows in Fig. 2). In addition, the methods with temporal consistency (i.e. $l_{2,1}$ and proposed methods) introduce more structural details of

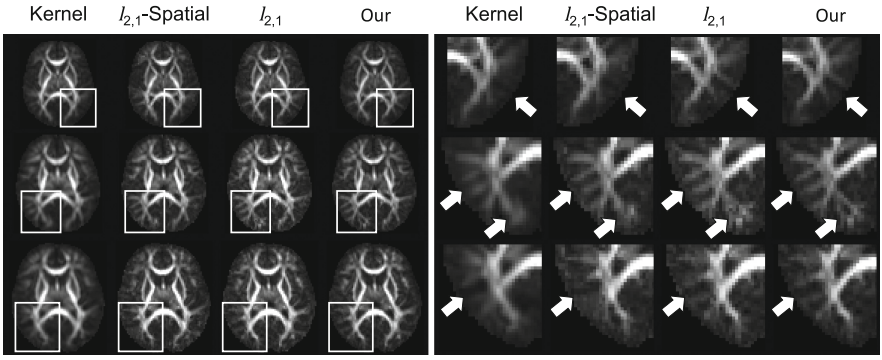

Fig. 2. Fractionial anisotropy maps of diffusion-weighted atlases, generated by kernel regression using age (Kernel), muti-task LASSO with spatial consistency ($l_{2,1}$-Spatial), multi-task LASSO with spatiotemporal consistency ($l_{2,1}$), and the proposed method (Our). Compared with other methods, the proposed method provides more details with less artifacts in longitudinal atlases (see arrows in right columns). 1st row: neonate; 2nd row: 6 months; 3rd row: 12 months.

infant brain, which are more consistent between the atlases at different ages. The effectiveness of our method is further supported by Fig. 3, which shows the orientation distribution functions (ODFs) of the atlases. In the atlas given the kernel regression method, many ODFs in cerebral cortex are missing due to the lower anisotropy. Compared with the atlases of the $l_{2,1}$-Spatial and $l_{2,1}$ methods, the proposed atlas shows more coherent ODFs along white matter (WM) with less spurious peaks (see arrows in Fig. 3). Figure 4 shows the fiber tracts of the splenium of the corpus callosum, which are extracted from the atlases. Seeds were assigned to the middle of the splenium. The atlases given by the kernel regression and $l_{2,1}$-Spatial methods produces larger bundles with less number of branches. The proposed atlas gives more well-connected fiber tracts with clearly separated branches, compared with the atlas given by the $l_{2,1}$ method (see arrows in Fig. 4). Figure 5 shows the tracts that traverse the corpus callosum in the atlases of the proposed method at birth and 6 months and 12 months of age.

3.4 Evaluation of Temporal Consistency

We assess the temporal consistency of the atlases in terms of fiber tract consistency of across time points. We assume that longitudinal DW atlases with more temporally consistent features can yield less distortion in propagating individual images at a time point to different temporal spaces via the atlases. For this purpose, we first obtain fiber tracts, including inferior fronto-occipital fasciculus (IFOF), forceps minor (F-Minor), and hand-superior U-tract (U-Tract), from the testing DW images at the neonatal time point. Then, we transform the fiber tracts from the individual neonatal space to the space of the same individual at later time points in two ways:

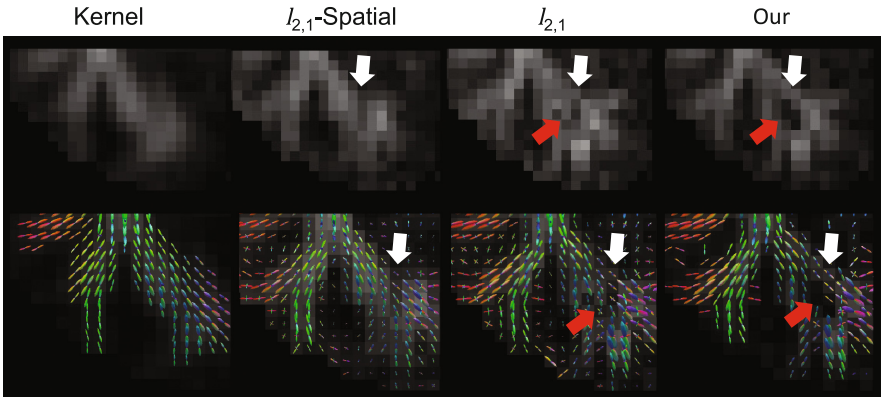

Fig. 3. Orientation distribution functions (ODFs) of diffusion-weighted atlases at 6 months of age, generated by kernel regression using age (Kernel), muti-task LASSO with spatial consistency ($l_{2,1}$-Spatial), multi-task LASSO with spati-temporal consistency ($l_{2,1}$), and the proposed method (Our). The proposed method provides ODFs with coherent fiber orientation along the white matter to the cerebral cortex.

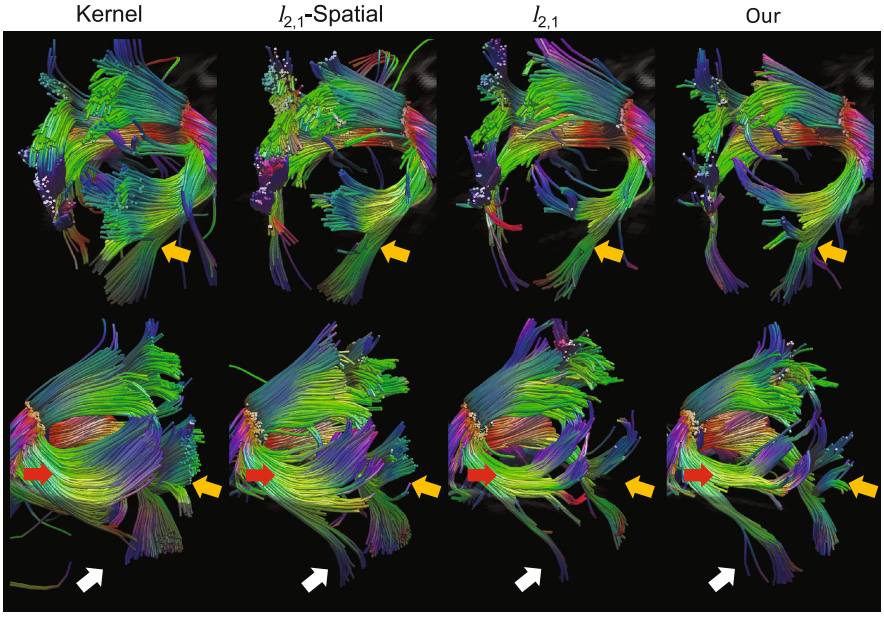

Fig. 4. Fiber tracts of the splenium of corpus callosum, extracted from diffusion-weighted atlases at 6 months of age. The proposed atlas provides more clearly separated branches and well-connected tracts to the cerebral cortex. Kernel: kernel regression using age; $l_{2,1}$-Spatial: muti-task LASSO with spatial consistency; $l_{2,1}$: multi-task LASSO with spati-temporal consistency; Our: the proposed method. 1st row: right side of the splenium; 2nd row: left side of the splenium.

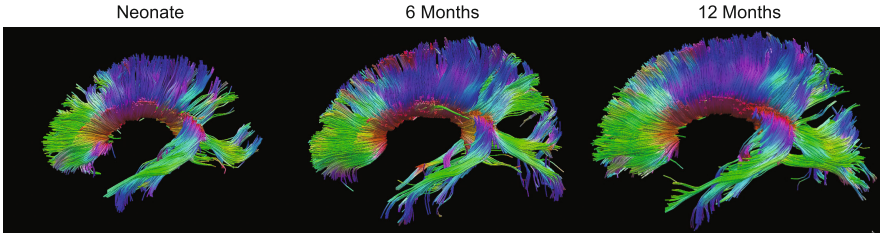

Fig. 5. Tracts that traverse the corpus callosum, extracted from the diffusion-weighted atlases generated by the proposed method at neonate, 6 months, and 12 months of age.

(A) Direct transformation from the testing images at the neonatal time point to the DW images of the same subjects at later time points (i.e., 6 and 12 months).
(B) Atlas-guided transformation (1) from the testing images to the neonatal atlases, (2) from the neonatal atlases to the atlases of later time points, and (3) from the atlases to the testing images at later time points.

The non-linear transformations are obtained by affine transformation followed by diffeomorphic non-linear registration using the FA maps of the atlases and the testing images. Transformation using method (A) is relatively small and can be estimated very reliably. Hence it is used as the baseline for comparison. The transformed tracts are compared using symmetric mean distance over all closest point pairs. Figure 6 shows the average of the mean distances between the fiber tracts for 8 testing subjects. The small distances given by the proposed method indicate that the atlases generated by it are more temporally consistent.

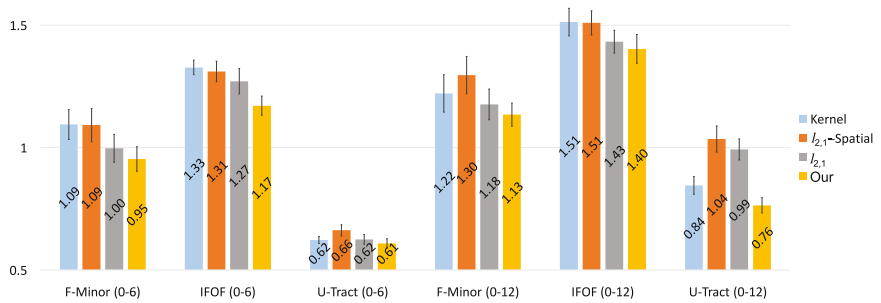

Fig. 6. Mean distances between fiber tracts, transformed by displacement between individual brains at different ages and displacement between longitudinal atlases. F-Minor: forceps minor; IFOF: inferior fronto-occipital fasciculus; U-Tract: hand-superior U-tract. 0–6: propagation from neonate to 6 months; 0–12: from neonate to 12 months.

4 Conclusion

In this paper, we have introduced a novel method based on graph-constrained sparse reconstruction for constructing longitudinal DW atlases of the developing infant brain in a patch-wise manner. Our method results in the atlases with more structural details, less artifacts, and greater temporal consistency.

Acknowledgments. This work was supported in part by an NIH grants (1U01MH110274, NS093842, and EB022880) and the efforts of the UNC/UMN Baby Connectome Project Consortium.

References

1. Qiu, A., Mori, S., Miller, M.I.: Diffusion tensor imaging for understanding brain development in early life. Annual Rev. Psychol. **66**(1), 853–876 (2015)
2. Oishi, K., Mori, S., Donohue, P.K., Ernst, T., Anderson, L., Buchthal, S., Faria, A., Jiang, H., Li, X., Miller, M.I., van Zijl, P.C.M., Chang, L.: Multi-contrast human neonatal brain atlas: application to normal neonate development analysis. NeuroImage **56**(1), 8–20 (2011)
3. Yeh, F.C., Tseng, W.Y.I.: NTU-90: A high angular resolution brain atlas constructed by Q-space diffeomorphic reconstruction. NeuroImage **58**(1), 91–99 (2011)
4. Serag, A., Aljabar, P., Ball, G., Counsell, S.J., Boardman, J.P., Rutherford, M.A., Edwards, A.D., Hajnal, J.V., Rueckert, D.: Construction of a consistent high-definition spatio-temporal atlas of the developing brain using adaptive kernel regression. NeuroImage **59**(3), 2255–2265 (2012)
5. Shi, F., Wang, L., Wu, G., Li, G., Gilmore, J.H., Lin, W., Shen, D.: Neonatal atlas construction using sparse representation. Hum. Brain Mapp. **35**(9), 4663–4677 (2014)
6. Tibshirani, R.: Regression shrinkage and selection via the lasso. J. R. Stat. Soc. Ser. B **58**, 267–288 (1996). (Methodological)
7. Zhang, Y., Shi, F., Wu, G., Wang, L., Yap, P.T., Shen, D.: Consistent spatial-temporal longitudinal atlas construction for developing infant brains. IEEE Trans. Med. Imag. **35**(12), 2568–2577 (2016)
8. Zhang, Y., Shi, F., Yap, P.T., Shen, D.: Detail-preserving construction of neonatal brain atlases in space-frequency domain. Hum. Brain Mapp. **37**(6), 2133–2150 (2016)
9. Saghafi, B., Chen, G., Shi, F., Yap, P.-T., Shen, D.: Construction of neonatal diffusion atlases via spatio-angular consistency. In: Wu, G., Coupé, P., Zhan, Y., Munsell, B.C., Rueckert, D. (eds.) Patch-MI 2016. LNCS, vol. 9993, pp. 9–16. Springer, Cham (2016). doi:10.1007/978-3-319-47118-1_2
10. Li, C., Li, H.: Network-constrained regularization and variable selection for analysis of genomic data. Bioinformatics **24**(9), 1175–1182 (2008). (Oxford, England)
11. Joshi, S., Davis, B., Jomier, M., Gerig, G.: Unbiased diffeomorphic atlas construction for computational anatomy. NeuroImage **23**(Suppl 1), S151–60 (2004)
12. Chen, G., Zhang, P., Li, K., Wee, C.Y., Wu, Y., Shen, D., Yap, P.T.: Improving estimation of fiber orientations in diffusion MRI using inter-subject information sharing. Sci. Rep. **6**, 37847 (2016)
13. Jenkinson, M., Beckmann, C.F., Behrens, T.E.J., Woolrich, M.W., Smith, S.M.: FSL. NeuroImage **62**(2), 782–790 (2012)